Journal of Fluorescence, Vol. 6, No. 2, 1996

Development of a Laser-Based Fluorescence Microscope with Subnanosecond Time Resolution

A. D. Scully,[1,4,5] A. J. MacRobert,[2] S. Botchway,[3] P. O'Neill,[3] A. W. Parker,[1] R. B. Ostler,[4] and D. Phillips[4]

Received September 11, 1995; accepted April 23, 1996

This report describes the development of a fluorescence microscope based on a standard inverted optical microscope which incorporates a pulsed picosecond dye laser excitation source and a detector consisting of a gated image intensifier coupled to a CCD camera. Fluorescence images have been obtained using gate durations of 0.5 ns from this apparatus, representing a reduction in gate duration of an order of magnitude compared with similar instruments reported by others recently. Subnanosecond gated fluorescence images of V79-4 Chinese hamster lung fibroblasts stained with a phthalocyanine photosensitizer used in photodynamic therapy are presented. The results of these measurements are discussed in terms of the intracellular distribution of the sensitizer. Other potential applications and limitations of this technique are also outlined.

KEY WORDS: Subnanosecond fluorescence microscopy; fluorescence lifetime mapping; phthalocyanine photosensitizer.

INTRODUCTION

One of the most rapidly developing areas in the field of photomedicine over the past 10 years has been the exploration of the use of light-activated molecules, known as photosensitizers, in the selective destruction of malignant tumors.[1] The photosensitizers are retained preferentially in the malignant tumour cells and upon irradiation with red light (600–800 nm) generate cytotoxic species, such as singlet oxygen, which are believed to react with and destroy local tissue.[1] This treatment, called photodynamic therapy (PDT), is currently undergoing clinical trials.[2,3] Among the most promising photosensitizers for PDT is disulfonated aluminium phthalocyanine (AlSPc), which has been studied extensively over the last 5 years.[4–8] The photoproperties of AlSPc which make it a particularly attractive candidate for use as a PDT sensitizer are (i) a large extinction coefficient in the far red end of the visible spectrum; (ii) a high yield of a relatively long-lived excited triplet-state species, thereby ensuring efficient generation of cytotoxic species; and (iii) a sufficiently high fluorescence quantum yield to enable *in vivo* detection.

A knowledge of the distribution of sensitizers in cells and tissues is essential for improvement in understanding of the photosensitization mechanism and the determination of optimal treatment times and dosimetry. The intrinsic fluorescence from AlSPc provides a convenient means of probing its intracellular localization. Investigations of the intracellular localization of sensitizers using steady-state fluorescence imaging microscopy[4,6,7,9,10] have relied on the assumption that the

[1] Central Laser Facility, Rutherford Appleton Laboratory, Chilton, U.K.
[2] National Medical Laser Centre, University College London Medical School, London, U.K.
[3] MRC Radiobiology Unit, Chilton, U.K.
[4] Department of Chemistry, Imperial College of Science, Technology and Medicine, London, U.K.
[5] To whom correspondence should be addressed at Lasers *for* Science Facility, Rutherford Appleton Laboratory, Chilton, Didcot, Oxon OX11 0QX, U.K.

1053-0509/96/0600-0119$09.50/0

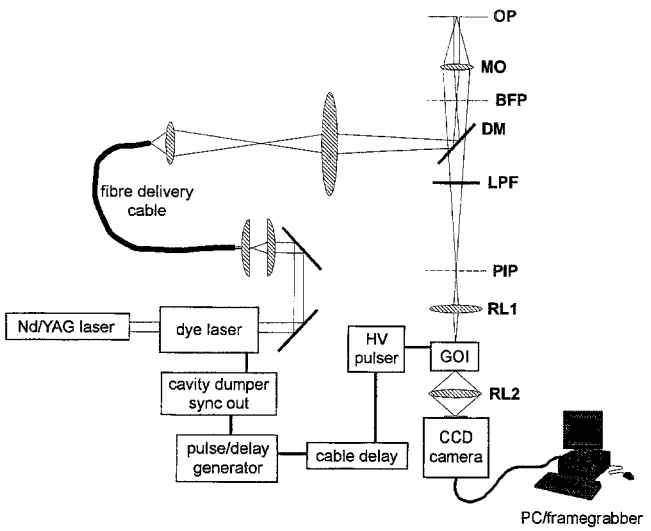

Fig. 1. Schematic diagram of the fluorescence microscope developed in this work. OP, object plane; MO, microscope objective lens; BFP, back focal plane of objective lens; DM, dichroic mirror; LPF, long-pass filter; PIP, primary image plane of microscope; RL1 and 2, relay lenses; GOI, gated optical image intensifier; CCD, 8-bit video rate camera.

distribution of fluorescence intensity provides an accurate representation of the intracellular concentration distribution of the sensitizer. However, the intensity of fluorescence from fluorophores is often found to be a function of the nature of its local environment. Chemical and physical properties of the environment such as polarity, pH, oxygen concentration, and interactions between the fluorophore and specific ionic species can have a pronounced effect on the intrinsic fluorescence decay time of the fluorophore,[11] and this in turn affects the intensity of the steady-state fluorescence emission. Furthermore, aggregation of the fluorescent sensitizer may result in the formation of a species that has significantly different fluorescent properties to the monomer.[12] It is not possible to account for these effects using steady-state fluorescence imaging microscopy.

Fluorescence lifetime imaging microscopy provides a solution to these problems.[11,13–28] The main feature of fluorescence lifetime measurements is that lifetimes are usually independent of probe concentration, photobleaching, and other artifacts affecting fluorescence intensity measurements. Time-resolved fluorescence detection can thus be used to determine fluorescence lifetime maps which are necessary for determination of the true spatial distribution of a probe molecule. Moreover, it can enhance contrast between the fluorescence arising from distributions of different probe species with similar spectral characteristics and provides a means of discriminating against background autofluorescence. Time-resolved fluorescence imaging can also be used to facilitate the monitoring of the intracellular concentrations of physiologically important ions such as H^+ and Ca^{2+}[13–16,21,22,28] by excitation of a single fluorescence probe molecule at a single excitation wavelength and detection of the fluorescence signal over a single emission wavelength range, thereby simplifying the spectral requirements of the probe and complexity of the instrumentation.

In this work we report on the development of a fluorescence microscope having subnanosecond time resolution imaging capabilities. This is achieved through the use of a detector that is capable of greater than an order of magnitude shorter gate duration than detectors used in other comparable apparatus reported to date. Results obtained using this apparatus for the measurement of the intracellular distribution of AlSPc in V79-4 mammalian cells are presented. These results are believed to constitute the first reported subnanosecond gated fluorescence microscope images and open the way for higher-precision measurements of intracellular phenomena using fluorescent probes.

EXPERIMENTAL TECHNIQUES

Fluorescence Microscope

A schematic diagram of the fluorescence microscope is shown in Fig. 1. The excitation source consists of a cavity-dumped dye laser (Spectra Physics, Model 3500) that is pumped synchronously by a mode-locked Nd^{3+}/YAG laser (Spectron, Model SL903). The duration of the dye laser pulses is approximately 10 ps. The excitation wavelength used in this work was 610 nm and the dye laser pulse repetition rate was 0.8 kHz. The dye laser pulses were directed to the port of an inverted microscope (Olympus, IMT-2) using a 1-mm-diameter PMMA fiber-optic cable (Toray), the output of which was magnified and imaged in the back focal plane of the microscope objective lens. The microscope was fitted with a dichroic mirror (Omega Optical, 670DRLP02) and a long-pass filter (Schott, RG665).

The detector is comprised of an 18-mm-diameter gated optical image intensifier (GOI) (Kentech Instruments, Didcot, U.K.) capable of gate durations ranging from ~120 ps to ~1 ns, and a luminous gain of $\sim 10^3$ in a single-stage microchannel plate. Further details of this device have been published previously.[29] The sync out signal from the cavity dumper driver is routed to the pulse/delay generator (Farnell), which supplies the trig-

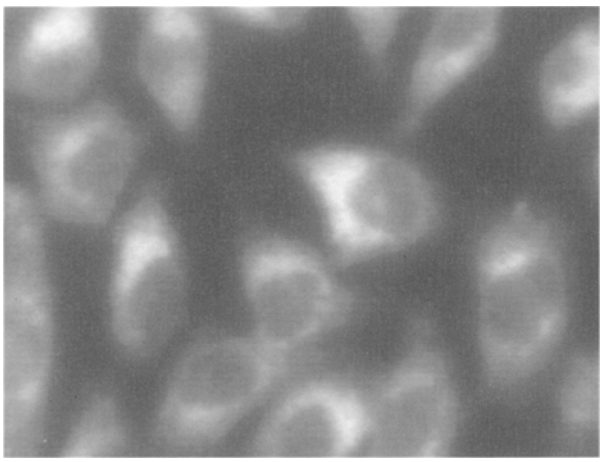

Fig. 2. Fluorescence intensity image of V79-4 Chinese Hamster lung fibroblasts stained with AlSPc obtained with GOI operating in DC mode. Image width = 110 μm; aspect ratio = 4:3.

ger signal to the GOI high-voltage pulser module *via* a switchable cable delay unit that is capable of introducing minimum incremental delays of 0.5 ns into the timing of the GOI trigger pulse. Iris effects, which may result from the periphery of the cathode turning on prior to the central region, and *vice versa*, on turning off,[30] have been minimized in the GOI by use of a mesh underlay that is capacitively coupled to the cathode. Iris effects would be expected to result in enhancement in brightness around the periphery of a gated image. The microscope field in the apparatus described in our work is imaged so as to illuminate a diameter of ~16 mm on the cathode and there is no detectable iris effect over this area when imaging fluorescence from a homogeneous solution placed on the microscope stage. The phosphor output of the GOI is coupled using a f/0.85 camera lens (Fujinon, CF25L) to the chip of an 8-bit scientific-grade CCD camera (Cohu, 4910) capable of on-chip integration times of tens of seconds at room temperature. Camera control is performed using a commercial framegrabber package (Oxford Framestore Applications). All images presented here were measured using a Nikon 60× oil immersion (NA 1.4) microscope objective and represent a field width of 110 μm.

Sample Preparation

AlSPc was prepared using the same procedure as described elsewhere.[5] The V79-4 Chinese hamster lung fibroblasts were used due to their ability to form uniform monolayers and were grown and maintained at the MRC Radiobiology Unit.[31] Cells were allowed to grow as a monolayer in the presence of minimal essential medium (MEM), 10% (ICN Chemicals), 10% fetal calf serum (Sigma Biochemicals), 1% penicillin, and supplemented with 1% L-glutamine on the base of a petri dish having a 22-mm-diameter coverslip base over a period of 40 h in a humidified 5% CO_2 incubator at 310 K to allow the cells to flatten. These cells were then incubated with AlSPc in MEM for 2 h at 310 K. The concentration of AlSPc in the medium was 10 μM. The V79-4 cells were washed thoroughly with phosphate buffer solution prior to measurements.

RESULTS AND DISCUSSION

A steady-state fluorescence intensity image of V79-4 cells is shown in Fig. 2. The cellular uptake of the sensitizer is seen clearly in this figure, with significantly higher fluorescence intensity observed in the perinuclear regions than in the nucleus. A similar pattern of inhomogeneous intracellular spatial distribution of fluorescence intensity was reported recently[4,7] for leukaemic K562 cells. It has been proposed[32,33] that AlSPc selectively partitions into lysosomal membranes, mitochondria, and the Golgi apparatus. However, fluorescence intensity images alone are insufficient for discrimination between the effects of inhomogeneous sensitizer localization and localized quenching on the overall fluorescence intensity map. Time-resolved fluorescence imaging is required in order to distinguish between these two effects.

Figure 3 shows four sequential subnanosecond time-gated images of the same cells shown in Fig. 2, the fluorescence intensities having been scaled so as to fill the available grey levels. These images were obtained after on-chip integration of 750 video frames and represent 0.5-ns time windows in the decay profile of AlSPc. The spatial distribution of fluorescence intensity remains unchanged up to 7.5 ns after excitation and is essentially identical to that observed in the steady-state fluorescence intensity image shown in Fig. 2. The independence of the fluorescence lifetime of AlSPc on intracellular distribution can be inferred from these results. This is borne out by the lack of any corresponding spatial variation in fluorescence lifetime, as illustrated in the fluorescence lifetime map shown in Fig. 4.

Wang *et al.*[26] have shown that the fluorescence lifetime at any position, $\tau(x, y)$, can be calculated using the following equation, provided that the fluorescence signal at that position follows an exponentially decaying function:

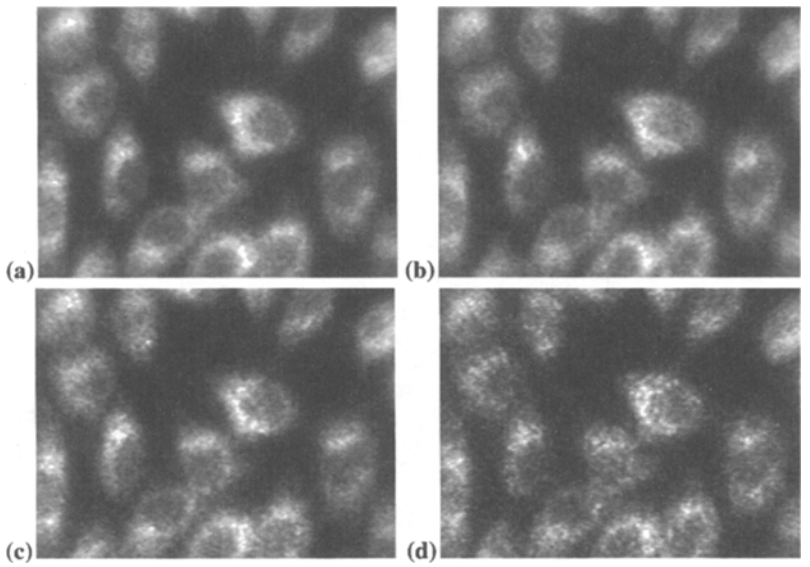

Fig. 3. Gated fluorescence images of the same cells as those shown in Fig. 2 measured using a gate width of 0.5 ns. Delay after time zero is (a) 0.5 ns, (b) 2.5 ns, (c) 5.0 ns, and (d) 7.5 ns. Each image was recorded using an integration time of 30 s (750 video frames) and has been scaled so as to fill the available gray levels.

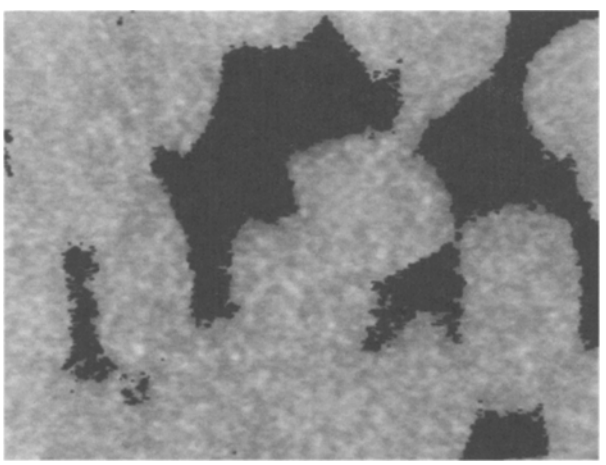

Fig. 4. Fluorescence lifetime map calculated by performing a linear least-squares analysis of the intensities measured at each image pixel of six gated fluorescence images.

$$\tau(x,y) = \frac{t_2 - t_1}{\ln\left[D_{t_1}(x,y) \Big/ D_{t_2}(x,y)\right]} \tag{1}$$

The parameters t_1 and t_2 are the delay times and $D_{t_1}(x, y)$ and $D_{t_2}(x, y)$ are the measured intensities associated with each gated fluorescence image. It can be seen from Eq. (1) that, in principle, the resolution with which the magnitude of $\tau(x, y)$ can be determined is not limited by the gate duration. A more precise estimate[34] of the fluorescence lifetime associated with a signal decaying according to the exponential function,

$$I_t(x,y) = A(x,y)\exp\left(\frac{-t}{\tau(x,y)}\right) \tag{2}$$

can be obtained by linear least-squares analysis according to Eq. (3) of the integrated intensities measured at several delay times along the fluorescence decay profile.

$$\ln[D_t(x,y)] = \ln B(x,y) - \frac{t}{\tau(x,y)} \tag{3}$$

where $B = A\tau\{1-\exp(-\Delta T/\tau)\}$ and ΔT is the gate duration, which is constant for each image. The fluorescence lifetime map shown in Fig. 4 was generated by calculating the apparent fluorescence decay time at each pixel from images collected at 0.5, 1.5, 2.5, 5.0, 7.5, and 9.0 ns after arrival of the excitation pulse at the sample using a linear least-squares analysis. The plots shown in Fig. 5 represent cross sections through the center of the lifetime map and provide more quantitative evidence for the independence of the fluorescence lifetime of AlSPc on its location within the cell. Therefore, the spatial distribution observed in the steady-state fluorescence image is Fig. 2 is attributed to a genuine distribution of AlSPc concentration within the cells. This type of analysis can also be applied to experiments involving the study of

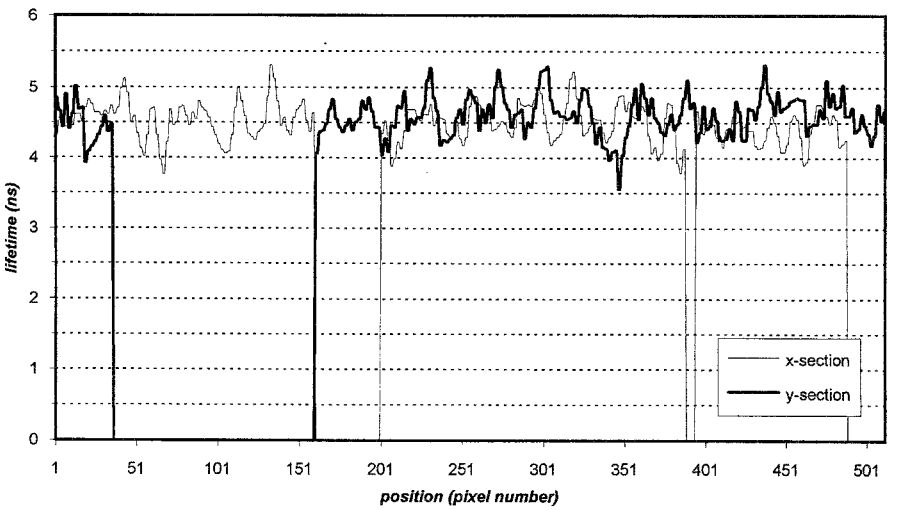

Fig. 5. Plots of the cross sections through the lifetime map, where x-section and y-section refer to sections taken through the center of the image in Fig. 4. Uncertainties in the lifetimes are estimated to be ~13%.

variations in the apparent intracellular fluorescence lifetime irrespective of whether or not the actual decay function at any particular image pixel is more complex than monoexponential, provided that a suitable calibration has been performed.

The fluorescence lifetime of ~4.5 ns obtained in this work for AlSPc in V79-4 cells is similar to values reported[4] for this molecule in PBS buffer solution. The fluorescence decay of AlSPc in K562 cells has recently been measured using the technique of time-correlated single-photon counting (TCSPC).[4] Analysis of the decay profiles measured from the most fluorescent areas of 15 cells required the use of a function based on the sum of two exponential components to fit the data satisfactorily. The best-fit decay times were determined to be 2.2 ± 0.4 and 6.1 ± 0.2 ns, with the preexponential factors being similar for each component. The best-fit exponential decay time, τ, for the fluorescence from AlSPc in K562 cells was estimated in order to enable comparison with the magnitude of τ determined from the lifetime map shown in Fig. 4. The values of the fluorescence intensity, I_t, at times corresponding to the six delay times, t, used in the present work were subjected to linear least-squares analysis according to the function shown in Eq. (4). The parameters τ_i and A' are the reported decay times and preexponential factors, respectively, where the preexponential factors were assumed to be the same for each exponential component.[4]

$$\ln(I_t) = \ln A - \frac{t}{\tau} \qquad (4)$$

where $I_t = A' \sum_{i=1}^{2} \exp(-t/\tau_i)$ and A is the preexponential factor associated with the monoexponential function. The value for τ of 4.4 ± 0.1 ns calculated from this analysis is in good agreement with the data shown in Fig. 5, which represent the fluorescence lifetime associated with the best-fit single-exponential decay through the six data points at each pixel.

The use of a gated intensifier capable of minimum gate widths of ~3 ns to generate fluorescence lifetime maps based on this type of analysis has been reported recently.[25–27] The time resolution of time-gated fluorescence measurements is limited by the jitter in timing of the triggering of the GOI, which is made up of contributions principally derived from the electronics in the GOI high-voltage pulser unit and the pulse/delay generator. The peak-to-peak jitter associated with both the pulser unit[26] and the delay generator[35] used in these recent studies is estimated to be of the order of 200 ps. This places an upper limit on the uncertainty in the timing associated with any delay time of approximately ±0.1 ns. If it is assumed that this is the only source of uncertainty involved, then the value of $\tau(x, y)$ must exceed ~1.5 ns in order to achieve an uncertainty of ≤10%. This places an undesirable restriction on the range of fluorescent probes suitable for the generation of fluorescence lifetime maps having sufficient precision to determine subtle variations in intracellular properties, such as ion concentrations. The peak-to-peak jitter of the intensifier used in the apparatus described in the present work is ≤40 ps, and the combined jitter of the cavity

dumper sync out and pulse/delay generator signal is estimated to be ~400 ps. However, with the use of a low-jitter digital pulse/delay generator (Kentech Instruments), acquired since the measurements reported here were made, the latter value has now been reduced to <100 ps. This places an upper limit of approximately 140 ps on the total peak-to-peak jitter associated with the timing of any image. Consequently, this apparatus has the potential to measure with acceptable precision apparent fluorescence lifetimes that are significantly shorter than 1 ns and to detect the presence of multiexponential fluorescence decay behavior.

Multiexponential functions are usually used for the analysis of the complex, nonexponential fluorescence decay profiles often obtained for fluorescent probes in biological systems.[4,36,37] Furthermore, most measurements of multiexponential fluorescence decay profiles using TCSPC are performed on a single-point basis and so generally offer only site-specific information. The detection of multiexponential fluorescence decay characteristics is not a requisite for the determination of intracellular perturbations on the fluorescence lifetime of a fluorescence probe, and in many cases it is sufficient to monitor variations in the *apparent* intracellular lifetime through the use of a fluorescence lifetime map. However, such information is necessary for a distinction to be made between effects such as quenching of the excited state and the presence of contributions by multiple fluorescent components. Wang *et al.*[25] have attempted to address the problem of detection of these more subtle effects on the fluorescence decay characteristics from gated fluorescence images by devising a method of image analysis that involves calculation of the ratio of early and late gated images and using the presence of plateau regions in the subsequent ratio image to determine the number of fluorescing components. The potential application of this method to time-resolved fluorescence microscopy was demonstrated[25–27] using a macroscopic test sample consisting of two differently shaped, overlapping polymer sections, each containing a fluorophore with a different fluorescence decay time. However, the use of this method in the analysis of fluorescence microscope images has not been reported, and it is not clear whether unambiguous results would be obtained for biological systems in which there may be a high spatial frequency in the variation of contributions of multiple fluorescent components to the overall fluorescence signal.

A more direct approach involves the measurement of time-gated images at several times along the fluorescence decay profile. This requires the use of gate durations that are short on the time scale of the fluorescence decay to be measured and minimal jitter in the timing of the gates. The intensity at any particular time and image location, $I_t(x, y)$, of a fluorescence signal that decays biexponentially can be described according to the function

$$I_t(x,y) = A_1(x,y)\exp\left(\frac{-t}{\tau_1(x,y)}\right) + A_2(x,y)\exp\left(\frac{-t}{\tau_2(x,y)}\right) \quad (5)$$

In this case, the integrated intensities measured at any particular delay time and spatial location, $D_t(x, y)$, also follows a biexponential decay function [Eq. (6)].

$$D_t(x,y) = C(x,y)\exp\left(\frac{-t}{\tau_1(x,y)}\right) + D(x,y)\exp\left(\frac{-t}{\tau_2(x,y)}\right) \quad (6)$$

where $C = A_1\tau_1\{1-\exp(-\Delta T/\tau_1)\}$, and $D = A_2\tau_2\{1 - \exp(-\Delta T/\tau_2)\}$. Nonlinear least-squares analysis of the integrated intensities measured at each pixel and delay time, $D_t(x, y)$ according to Eq. (6) will yield values for the two lifetimes at each pixel, $\tau_1(x, y)$ and $\tau_2(x, y)$. Deviations from exponential decay behavior should be detectable using this approach, provided a sufficiently large number of channels are collected and an adequate signal-to-noise ratio is attainable. The very short gate durations and low jitter associated with the intensifier used in the apparatus described here make this system ideally suited to such measurements and this is one aspect of further development to the apparatus that is currently being pursued.

ACKNOWLEDGMENTS

This work was supported financially by the EPSRC through Grant GR/J02094. We are grateful to K. M. S. Townsend of the MRC Radiobiology Unit for use of the microscope objective and the CLF staff for assistance with the lasers used in this work.

REFERENCES

1. R. Bonnett (1995) *Chem. Soc. Rev.* **24**, 19–33.
2. H.-B. Ris, H. J. Altermatt, R. Inderbitzi, R. Hess, B. Nachbur, J. C. M. Stewart, Q. Wang, C. K. Lim, R. Bonnett, M. C. Berenbaum, and U. Althaus (1991) *Br. J. Cancer* **64**, 1116–1120.
3. J.-F. Savary, P. Monnier, G. Wagnières, D. Braichotte, C. Fontolliet, and H. van den Bergh (1994) *Proc. SPIE* **2078**, 330–340.

4. M. Ambroz, A. J. MacRobert, J. Morgan, G. Rumbles, M. S. C. Foley, and D. Phillips (1994) *J. Photochem. Photobiol. B Biol.* **22**, 105–117.
5. M. Ambroz, A. J. MacRobert, M. S. C. Simpson, R. K. Steven, and D. Phillips (1991) *J. Photochem. Photobiol. B Biol.* **9**, 87–95.
6. W. S. Chan, A. J. MacRobert, D. Phillips, and I. R. Hart (1989) *Photochem. Photobiol.* **50**, 617–624.
7. A. J. MacRobert and D. Phillips (1990) *Proc. SPIE* **1439**, 79–87.
8. I. Rosenthal (1991) *Photochem. Photobiol.* **53**, 859–870.
9. H. Schneckenburger, A. Ruck, B. Bartos, and R. Steiner (1988) *J. Photochem. Photobiol. B Biol.* **2**, 355–363.
10. G. N. Georgiou, M. T. Ahmet, A. Houlton, J. Silver, and R. J. Cherry (1994) *Photochem. Photobiol.* **59**, 419–422.
11. J. R. Lakowicz, H. Szmacinski, K. Nowaczyk, and M. L. Johnson (1992) *Proc. Natl. Acad. Sci. USA* **89**, 1271–1275.
12. L. E. Bennett, K. P. Ghiggino, and R. W. Henderson (1989) *J. Photochem. Photobiol. B Biol.* **3**, 81–89.
13. J. R. Lakowicz (1992) *Laser Focus World* 1271–1275.
14. H. Scmacinski and J. R. Lakowicz (1993) *Anal. Chem.* **65**, 1668–1674.
15. J. R. Lakowicz, H. Szmacinski, and R. B. Thompson (1993) *Proc. SPIE* **1895**, 2–17.
16. J. R. Lakowicz and H. Szmacinski (1993) *Sensors Actuators B* **11**, 133–143.
17. R. Cubeddu, G. Canti, P. Taroni, and G. Valentini (1991) *Proc. SPIE,* **1525**, 17–25.
18. C. G. Morgan, A. C. Mitchell, and J. G. Murray (1991) *Proc. SPIE* **1525**, 83–90.
19. C. G. Morgan, J. G. Murray, and A. C. Mitchell (1990) *Proc. SPIE* **1204**, 798–807.
20. E. P. Buurman, R. Sanders, A. Draaijer, H. C. Gerritsen, J. J. F. van Veen, P. M. Houpt, and Y. K. Levine (1992) *Scanning* **14**, 155–159.
21. H. C. Gerritsen, R. Sanders, and A. Draaijer (1994) *Proc. SPIE* **2329**, 260–267.
22. R. Sanders, H. C. Gerritsen, A. Draaijer, P. M. Houpt, J. J. F. van Veen, and Y. K. Levine (1994) *Proc. SPIE* **2137**, 56–62.
23. X. F. Wang, T. Uchida, and S. Minami (1989) *Appl. Spectrosc.* **43**, 840–845.
24. X. F. Wang, S. Kitamura, T. Uchida, D. M. Coleman, and S. Minami (1990) *Appl. Spectrosc.* **44**, 25–30.
25. X. F. Wang, T. Uchida, M. Maeshima, and S. Minami (1991) *Appl. Spectrosc.* **45**, 560–565.
26. X. F. Wang, T. Uchida, D. M. Coleman, and S. Minami (1991) *Appl. Spectrosc.* **45**, 360–366.
27. X. F. Wang, T. Uchida, and S. Minami (1992) *Proc. SPIE* **1640**, 433–439.
28. X. F. Wang, A. Periasamy, G. W. Gordon, P. Wodnicki, and B. Herman (1994) *Proc. SPIE* **2137**, 64–76.
29. P. E. Young, J. D. Hares, J. D. Kilkenny, D. W. Phillion, and E. M. Campbell (1988) *Rev. Sci. Instrum.* **59**, 1457–1460.
30. S. Thomas, A. R. Shimkunas, and P. E. Mauger (1990) *Proc. SPIE* **1358**, 91–99.
31. J. Thacker, A. Stretch, and D. T. Goodhead (1982) Radiat. Res. **92**, 343–352.
32. Q. Peng, G. W. Farrants, K. Madslien, J. C. Bommer, J. Moan, H. E. Danielson, and J. M. Nesland (1991) *Int. J. Cancer* **49**, 290–295.
33. C. Tempete, C. Giabbotti, and G. H. Werner (1992) *J. Photochem. Photobiol. B Biol.* **14**, 201–205.
34. R. M. Ballew and J. N. Demas (1989) *Anal. Chem.* **61**, 30–33.
35. Stanford Research Systems (1987) DG535 delay/pulse generator operation and service manual, p. 7.
36. H. C. Gerritsen, C. J. R. van der Oord, Y. K. Levine, I. H. Munro, G. R. Jones, D. A. Shaw, and F. F. G. Rommerts (1994) *Proc. SPIE* **2137**, 238–242.
37. S. Hirayama (1992) in J. F. Rabek (Ed.), *Progress in Photochemistry and Photophysics Vol. 6*, CRC Press, Boca Raton, FL, pp. 1–42.